Understanding Hector: The Dynamics of Island Thunderstorms

N. ANDREW CROOK

National Center for Atmospheric Research, Boulder, Colorado*

(Manuscript received 30 March 2000, in final form 6 September 2000)

ABSTRACT

Linear and nonlinear models are used to examine the development of island thunderstorms, in particular the Hector convective system that forms over the Tiwi Islands just north of Australia. The linear model is used to examine the flow response to an isolated, elliptical, heat source. It is found that the low-level convergence is maximized when the flow is weak and along the major axis of the heat source. A dry version of the nonlinear model verifies the trends predicted by the linear model except at very low flow speeds where the convergence is bounded in the nonlinear model but increases indefinitely in the linear model.

Deep convection develops over the heat source when a moisture profile with positive convective available potential energy (CAPE) is added to the nonlinear model. The sensitivity of the convective strength (defined by the accumulated rainfall and total condensate) to wind speed and direction, surface fluxes, and low-level moisture is then examined. It is shown that the strength increases as the wind speed decreases and as the wind direction turns toward the major axis of the island, in agreement with the prediction of increased low-level convergence from the linear and nonlinear dry models. Sensitivity experiments indicate that the convective strength increases as both the heat and moisture fluxes increase. The strength is more sensitive to the heat flux since this drives the large-scale convergence and sea breezes that generate convection. As the low-level moisture in the upstream sounding increases, the accumulated rainfall over the islands increases monotonically; however, the total condensate reaches a maximum at a CAPE of around 1500 J kg^{-1} and then decreases thereafter. It is shown that the low-level moisture is an important predictor of the form of convective development. Finally, simulations with a single coastline are performed to show that one of the reasons the Hector convective system is so strong is that it develops over an island where the land–sea circulation from all coastlines can contribute.

1. Introduction

Hector is the name given to a thunderstorm complex that develops regularly over the Tiwi Islands just north of mainland Australia during the transition season (Nov–Dec, Feb–Mar). The Tiwi's consist of two relatively flat islands (Melville in the east, Bathurst in the west), which together cover approximately 150 km in the east–west direction and 50 km in the north–south direction. Convective activity maximizes during the afternoon indicating the importance of diurnal heating. The storms, which are easily visible from Darwin 100 km to the south, are among the world's tallest often reaching a height of 20 km.

The regular occurrence of the storms over isolated, basically flat, terrain makes the islands an excellent testing ground for observational and modeling studies. The storms have been the subject of two recent field programs: Island Thunderstorm Experiment (ITEX) in 1988 (Skinner and Tapper 1994) and Maritime Continent Thunderstorm Experiment (MCTEX) in 1995 (Carbone et al. 2000). These field programs successfully characterized the structure of convection over the Tiwi Islands in various flow regimes. They also gave an idea of the functional relationship between convective strength and various external parameters, although the small sample size of the dataset limited the conclusions that could be drawn.

Numerical simulations of the Hector convective system have been performed by Golding (1993) and Saito et al. (2001). Golding (1993) used the U.K. Met. Office's mesoscale model at 3-km resolution to examine two cases from ITEX and was able to simulate the development of deep convection over the islands. The sensitivity of the simulated convection to resolution, island shape, and model microphysics was also explored. Saito et al. (2001) used the Japanese Meteorological Research Institute's mesoscale model at 1-km resolution to simulate an observed case from MCTEX. The sensitivity to microphysics, topography, and island size was also examined.

In this study we will concentrate on the mechanisms that control convective development over the islands.

* The National Center for Atmospheric Research is sponsored by the National Science Foundation.

Corresponding author address: Dr. N. Andrew Crook, NCAR, P.O. Box 3000, Boulder, CO 80307.
E-mail: crook@ucar.edu

Over the past decade there has been an evolving view concerning the modes of convective development. Prior to MCTEX, it was theorized that Hector or the largest thunderstorms were produced only after the collision of sea-breeze fronts from the north and south coasts. During MCTEX detailed observations of the sea breezes were possible with a sensitive Doppler radar and it was learned that the sea breezes seldom collided. This led Carbone et al. (2000) to propose a conceptual model for two modes of convective development. In the most frequent mode (type B) the strongest thunderstorms develop upon the interaction of one sea breeze and a gust front from earlier convection. Carbone et al. (2000) estimate that this mode of development is responsible for approximately 80% of Hectors. In the second, less frequent, mode (type A) Hector develops upon the collision of sea breezes from the north and south coasts. They hypothesize that this mode occurs when conditions are more stable, allowing sea breezes to progress farther inland before evaporatively cooled gust fronts develop and disrupt their progress. In this study we will perform simulations to examine this hypothesis.

Although Hector is one of the most predictable convective systems on Earth, there are still a large number of parameters that can effect its development. These include wind speed and direction, wind shear, convective available potential energy (CAPE), convective inhibition, sensible and latent heat fluxes, large-scale disturbances, microphysics, and radiation. An exhaustive study of the complete parameter regime is not possible in this paper, so we concentrate here on five parameters that have been shown to be important in previous observational studies. These parameters are wind speed and direction, surface fluxes of moisture and heat, and low-level moisture.

The outline of the paper is as follows: in section 2 a linear model of flow over an isolated heat source is developed to examine the dependence of the lifting on flow speed and direction and heating rate. These analytical results will help guide the nonlinear numerical simulations, which are described in section 3. These simulations will be used to determine the integrated convective response to the heating and cooling over the islands. Although these simulations will show the dependence of the convective strength on the low-level convergence, a complete dynamical explanation of this dependence is considered to be beyond the scope of the present study. Finally, section 4 summarizes the results and gives some concluding remarks.

2. Analytical model of flow over a heat source

As discussed in the introduction, the observation that storms form almost daily during the transition season and gain maximum intensity in the afternoon points to the importance of diurnal heating over the islands. In this section we examine a linear model of flow over an isolated heat source in order to gain insight into the effects of that heating. The linear response of an airflow to prescribed heating has been examined by a number of authors (e.g., Malkus and Stern 1953; Raymond 1972; Smith and Lin 1982; Lin 1986). In this study, we follow the work of Lin (1986) who developed a model of the three-dimensional response to an isolated heat source.

To simplify the analysis we assume that the flow is steady state, Boussinesq, and incompressible. We further assume that the upstream velocity, U, and Brunt–Väisälä frequency, N, are constant in the vertical. The governing equations for small-amplitude flow (u, v, w) forced by a heat source q are then

$$Uu_x = -\frac{p_x}{\overline{\rho}} - \nu u \tag{1}$$

$$Uv_x = -\frac{p_y}{\overline{\rho}} - \nu v \tag{2}$$

$$Uw_x = -\frac{p_z}{\overline{\rho}} - \frac{\rho}{\overline{\rho}}g - \nu w \tag{3}$$

$$U\rho_x - \frac{\overline{\rho}N^2}{g}w = -\frac{\overline{\rho}}{c_p\overline{T}}q - \nu\rho \tag{4}$$

$$u_x + v_y + w_z = 0. \tag{5}$$

The mean temperature and density of the environment are denoted by $\overline{T}$, $\overline{\rho}$ while the perturbation pressure and density are denoted by p, ρ, respectively, and ν is the coefficient of both the Rayleigh friction and Newtonian cooling and the other symbols have their usual meanings. Taking the Fourier transform in x and y, the governing equations can be written as

$$\hat{w}_{zz} + \frac{(N^2 - (Uk - i\nu)^2)\kappa^2}{(Uk - i\nu)^2}\hat{w} = \frac{g\kappa^2}{c_pT(Uk - i\nu)^2}\hat{q}, \tag{6}$$

where $\hat{w}$ and $\hat{q}$ are the Fourier components of w and q, respectively; $\kappa = (k^2 + l^2)^{1/2}$ and k and l are the wavenumbers in the x and y directions.

Equation (6) is solved for a heat source that is elliptically shaped in the horizontal in order to approximate the shape of the Tiwi Islands. It is assumed that the heat is applied uniformly in the vertical below a height $z = H$. The heat source has the following functional form:

$$q(x, y, z) = \begin{cases} \dfrac{Q_o}{1 + \dfrac{x^2}{L_x^2} + \dfrac{y^2}{L_y^2}} & \text{for } z \le H \\ 0 & \text{for } z > H. \end{cases} \tag{7}$$

Before examining solutions for the vertical velocity, we first perform a scale analysis of the wave equation (6). We assume that the circulation forced by the heat source has characteristic length scales of L_x, L_y in the horizontal and H in the vertical. The vertical velocity then scales as

$$w \propto \frac{gQ_o}{c_pTN^2}\frac{1}{1 + \mathrm{Fr}^2\left(\dfrac{L_y^2}{L_y^2 + L_x^2}\right)}, \tag{8}$$

where we have assumed $\nu = 0$. We have also made the hydrostatic assumption $U/NL_x \ll 1$, that is, that the horizontal scale of the flow, L_x, is large compared to the vertical scale, U/N. This assumption is valid for typical values of the flow over the Tiwi Islands. The Froude number is $\mathrm{Fr} = U/(NH)$, which measures the ratio of the flow speed U to the internal wave speed NH. The first point to note is that the vertical velocity is directly proportional to the heating rate Q_o. We now examine the response in two parameter regimes (low and high Froude numbers).

(a) $\mathrm{Fr} \ll 1$ high stability/low flow:
For low Froude number flow, (8) reduces to

$$w \propto \frac{gQ_o}{c_pTN^2}. \tag{9}$$

In this parameter regime, the vertical velocity is inversely proportional to the stability N^2 and independent of the flow U. The balance in the thermodynamic equation is between the heating q and the vertical advection of buoyancy.

(b) $\mathrm{Fr} \gg 1$ low stability/strong flow:
For high Froude numbers, (8) reduces to

$$w \propto \frac{gQ_oH^2}{c_pTU^2}\left(1 + \frac{L_x^2}{L_y^2}\right). \tag{10}$$

In this parameter regime, the vertical velocity is inversely proportional to U^2 and independent of the stability N^2. The balance in the thermodynamic equation is between the heating q and horizontal advection over the heat source. Equation (10) also indicates that the vertical velocity is greatest when $L_x > L_y$, which is the case where the flow is along the major axis of the heat source.

Determining the typical Froude number over the Tiwi Islands when strong convection develops is not straightforward because of the variation of N^2 with height. In the free troposphere, the stability N^2 is of the order of $1.0 \times 10^{-4}\ \mathrm{s}^{-2}$. However in the boundary layer, where the heat is being added, the stability is near zero. In the nonlinear simulations to be presented in section 3, the potential temperature increase across the boundary layer is of the order of 0.1°C while the depth of the well-mixed layer is approximately 1 km (giving an $N^2 \sim 3. \times 10^{-6}\ \mathrm{s}^{-2}$). For the flow speed, U, Carbone et al. (2000) found that all thunderstorm days during MCTEX had surface wind speeds less than 4 m s^{-1}. Using the estimates above for the stability and depth of the boundary layer gives a Froude number of 0.5 for a flow of 1 m s^{-1} and 2.0 for a flow of 4 m s^{-1}.

Although the above estimates are very qualitative they do suggest that the Froude number is of the order of one for typical flow conditions over the Tiwi Islands, neither in the high nor low limit. In this moderate Froude number range, the vertical velocity is dependent on both N and U, decreasing as both parameters increase.

Solutions to the wave equation (6) are now examined. Following the methodology of Lin (1986) the solution for w in the heating layer ($0 < z < H$) can be written

$$w = \frac{gb^3}{c_pTUN}\int_{-\infty}^{\infty}\int_{-\infty}^{\infty}\hat{q}[e^{i\lambda z}(\cos\lambda z - 1) + i\sin(\lambda z)(e^{i\lambda H} - e^{i\lambda z})]e^{i(kx+ly)}\,dk\,dl, \tag{11}$$

where $\lambda = N\kappa/Uk$. We now examine the dependence of the vertical velocity on the wind speed and direction relative to the heat source in (7). The maximum heating rate is set at 400 W m^{-2}, which is representative of the values observed around midday at this time of the year over the Tiwi Islands (Beringer et al. 1997). The depth H is taken as 1000 m, which is a typical depth of the boundary layer over the islands (Carbone et al. 2000). Thus $\rho Q_o = 400/1000\ \mathrm{W\ m^{-3}} = 0.4\ \mathrm{W\ m^{-3}}$. For the stability, N^2, we use the value of $N^2 = 3.3 \times 10^{-6}\ \mathrm{s}^{-2}$ from the numerical simulations of section 3.

Figure 1a shows the surface velocity vectors and the vertical velocity at the top of the heat source, $z = H$, with a flow of $U = 4$ m s^{-1} directed along the major axis of the heat source. As the flow passes over the heat source it converges toward the centerline (major axis) of the heat source. Consistent with this convergence is a band of vertical velocity in the downwind half of the island.

Figure 1b shows the response when the flow is along the minor axis of the heat source. (Note that we have rotated the heat source rather than the flow in this figure.) Again the flow converges toward the centerline (in this case, minor axis) of the heat source. A band of vertical velocity develops on the downwind side of the island. The maximum vertical velocity in this case is reduced by a factor of 3.5 compared to that in Fig. 1a.

Figure 1c shows the response when the flow is at an angle of 45° to the major axis. Again, the largest lifting occurs in the downwind side of the heat source with the amplitude between that shown in Figs. 1a and 1b.

Figure 2 shows the response to changes in flow speed. In Fig. 2b the flow is along the major axis of the heat source with a speed of 2.0 m s^{-1}. In this case the vertical

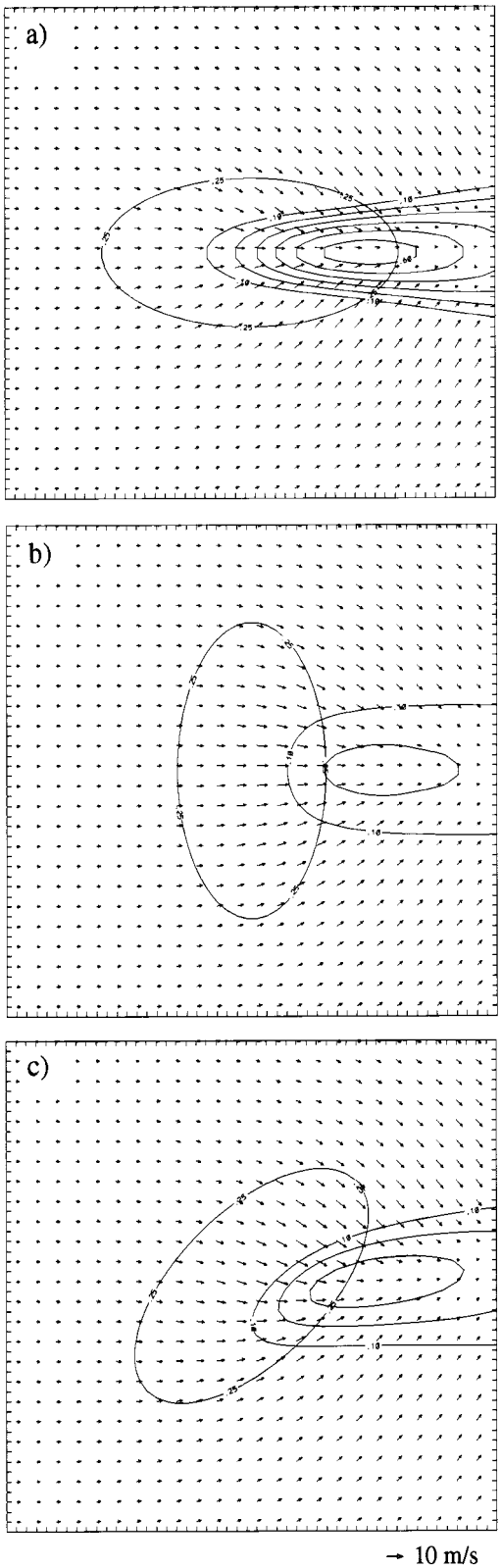

FIG. 1. Surface vectors and vertical velocity at the top of the heat source for flow of 4 m s^{-1} past an elliptical heat source. Contour interval for vertical velocity is 0.1 m s^{-1}. Thick contour bounds the region where the heating rate is >25% of the maximum. (a) Flow along major axis of heat source, (b) along minor axis, and (c) at 45° to major axis.

velocity is significantly increased by a factor of 2.2. In Fig. 2c the flow is increased to 8 m s^{-1} and the vertical velocity is reduced by a factor of 2.0. We note that although the vertical velocity does decrease as the flow speed U increases, the dependence does not follow that predicted in the high Froude number limit [proportional to $1/U^2$, Eq. (10)] since the Froude number for these calculations is only in the moderate range (Fr = 1 → 4).

The linear model described above has elucidated some of the characteristics of the large-scale circulation forced by an isolated heat source. As will be shown in the next section, the full nonlinear flow is significantly more complicated than that shown in Figs. 1 and 2. However, it is useful to keep this large-scale circulation in mind when viewing the more complex nonlinear simulations.

3. Numerical simulations

To explore the full nonlinear evolution of the flow over an isolated heat source we use the Clark, nonhydrostatic, anelastic model (Clark 1977). Subgrid-scale diffusion is parameterized using the first-order closure of Lilly (1962) and Smagorinsky (1963) (cf. Clark and Farley 1984). In the moist simulations, the Kessler (1969) warm rain and Koenig and Murray (1976) ice microphysical schemes are used. Radiation boundary conditions are used at all lateral boundaries. The surface fluxes of heat and moisture over the land are specified as constant (not a function of surface wind speed) and only vary with the time of day. A number of sensitivity tests will be performed with varying maximum (noontime) surface fluxes. The model domain is 220 km in the east–west direction and 120 km in the north–south direction with a horizontal resolution of 1 km. The vertical resolution is 40 m in the lowest 2 km stretching to 800 m at the model top (24 km).

As mentioned in the introduction, the numerical model will be used to examine the sensitivity of convection to wind speed and direction, surface fluxes, and low-level moisture. To facilitate these sensitivity tests it was decided to use an idealized sounding, see Fig. 3. The wind profile is typical of a westerly flow regime (Carbone et al. 2000). At the surface, the flow is westerly then changes to easterly between 2 and 6 km and then back to westerly above 6 km. In the experiments that examine the sensitivity to the surface flow speed, a constant value is added to (or subtracted from) the wind speed, thus keeping the vertical shear unchanged. Similarly, in the wind direction sensitivity experiments, the wind vector is kept unidirectional by turning the vector by a constant angle at all heights. Note that the analytical

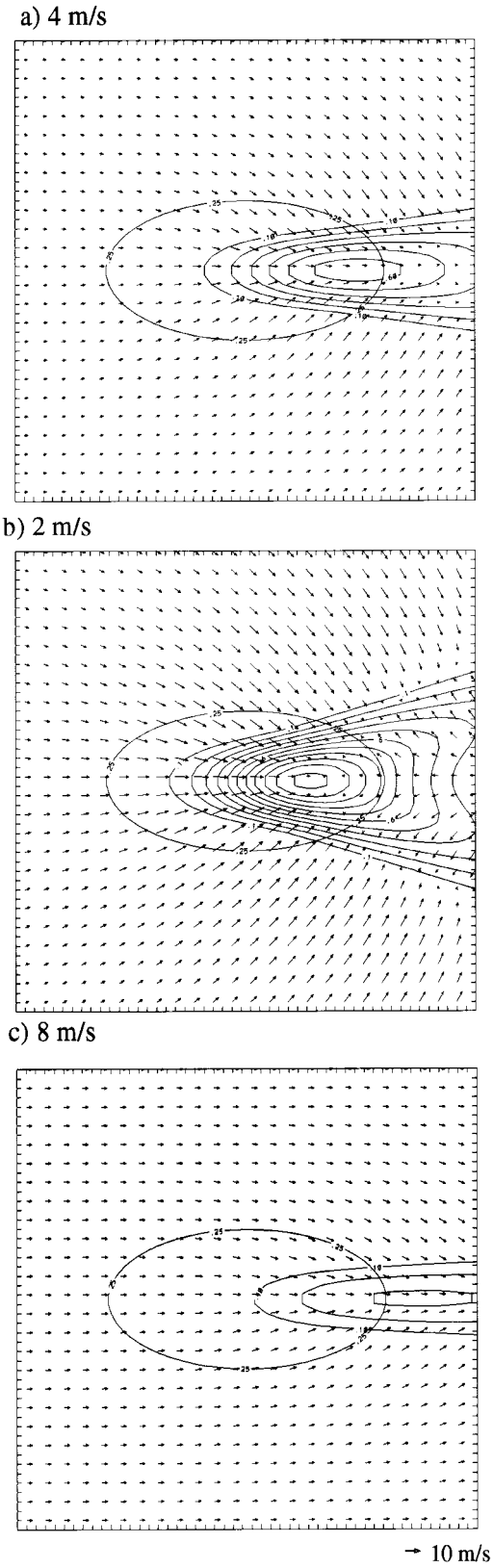

FIG. 2. Same as Fig. 1 except for varying flow speeds: (a) 4, (b) 2, and (c) 8 m s^{-1}.

solutions obtained in the previous sections were for an atmosphere with uniform upstream flow. To facilitate comparison with these solutions, simulations will also be performed with no shear in the upstream flow.

The temperature and moisture profile in Fig. 3 was obtained by smoothing an early morning sounding taken during MCTEX (28 Nov 1995). The control moisture is shown by the solid curve and has a surface value of 19.8 g kg^{-1} and a CAPE of 1500 J kg^{-1}. Two additional moisture profiles to be used in section 3b(5) are also plotted. The first has a CAPE of 1000 J kg^{-1} and a surface value of 18.2 g kg^{-1} (dotted line) and the second has a CAPE of 3000 J kg^{-1} and surface value of 21.2 g kg^{-1} (dashed line). The surface fluxes of sensible and latent heat are specified as a percentage of the incoming solar radiation for this latitude (11°S) and time of year. All of the simulations begin at 0700 local time.

a. Dry simulations

In order to describe the development of large-scale convergence and sea breezes over the Tiwi Islands, simulations without moisture were first performed. The control simulation has a surface flow speed of 4 m s^{-1} toward 90° (i.e., along the major axis of the islands). The latent heat flux is set to zero while the sensible heat flux is set at 40% of the incoming solar radiation. This value for the sensible heat flux is typical of that observed during MCTEX (Beringer et al. 1997). [The sensitivity to both the sensible and latent heat fluxes is examined in section 3b(4).] Figure 4 shows the surface wind vectors after 4 h of integration, 1100 LT. (Vectors are shown at every fourth grid point). Sea breezes from the north and south coastlines have moved approximately 15 km inland. Convective boundary layer eddies have developed over the heated land surface, between the two sea breezes.

The linear model described in the previous section is not able to capture nonlinear features such as sea breezes and convective eddies. The vertical velocities associated with these nonlinear features (of the order of meters per second) are also significantly larger than the vertical velocity associated with the large-scale convergence shown in Figs. 1 and 2. (of the order of centimeters per second). Nevertheless, the influence of the large-scale convergence can still be seen in the nonlinear simulations. To identify this large-scale convergence a passive tracer field was added at $t = 0$. The tracer was initially horizontally homogeneous with a value of one at the surface linearly decreasing to zero at a height of 3 km. The tracer field at 1100 LT and at a height of 1500 m is shown in Fig. 5a (surface velocity field overlaid). A band of increased tracer concentration can be seen in the downwind half of the island complex similar to that predicted by the linear model. An important point to note is that the tracer concentration is enhanced throughout the region between the two sea breezes and not just at the leading edge of the sea breezes. In other words,

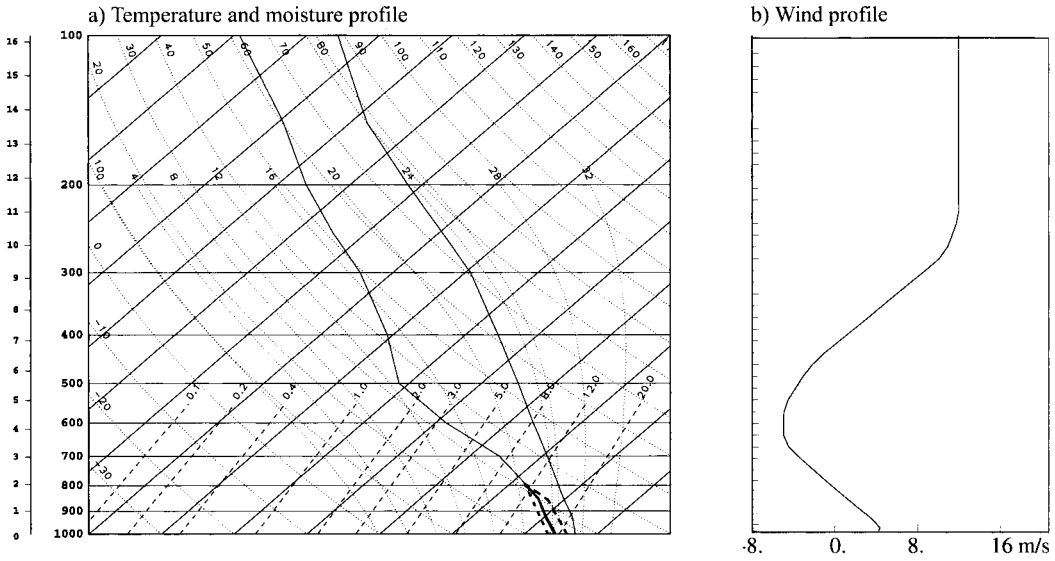

FIG. 3. (a) Temperature and moisture sounding used in the control experiment with the nonlinear model. Moisture profiles with CAPEs of 1000 J kg^{-1} (dotted) and 3000 J kg^{-1} (dashed) are also shown. (b) Wind profile.

large-scale lifting is occurring not just at the two sea-breeze fronts but throughout the region between the two breezes.

The large-scale lifting can also be seen in the buoyancy field. Figure 5b is a vertical profile of the buoyancy averaged over the islands. At low levels, the buoyancy has been increased by surface heating (by an average of 3°C at the surface); however, above the boundary layer, there is a layer of approximately 2000 m in thickness of negative buoyancy. On average, this negative buoyancy reaches a minimum of around −0.2°C, although there are local minima of −2.0°C. This cooling is caused by the large-scale lifting over the islands, which is important for destabilizing the atmosphere for the later development of convection.

To quantify this lifting, we plot the mean vertical velocity over the islands (integrated vertical velocity divided by the total area of the islands) as a function

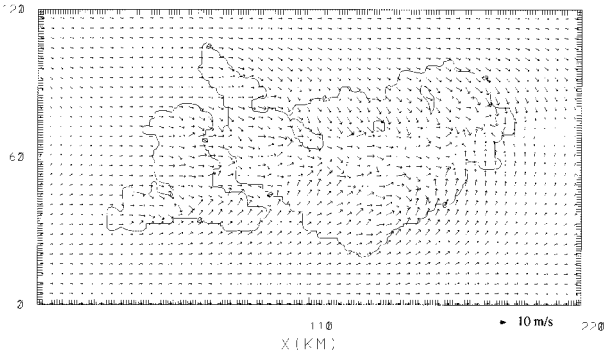

FIG. 4. Surface vectors at t = 1100 LT for a simulation without moisture and an upstream flow of 4 m s^{-1}. Vectors are shown at every fourth grid point. The coastline of the Tiwi Islands is shown by the solid contour.

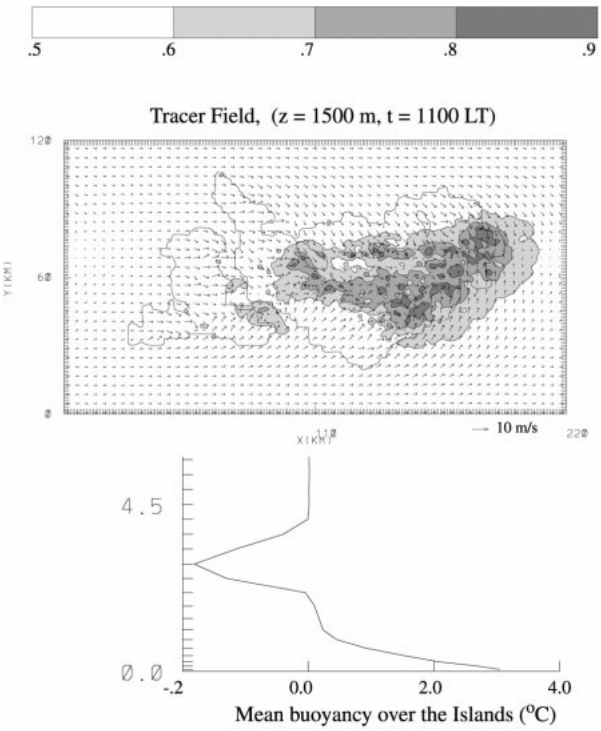

FIG. 5. (a) Concentration of tracer field at z = 1500 m overlaid on surface vector field (t = 1100 LT). Initially, the tracer field is horizontally homogenous with a value of one at the surface, linearly decreasing to zero at 3 km. (b) Vertical profile of mean buoyancy field above the Tiwi Islands. Note that the scale on the negative side has been expanded by a factor of 10.

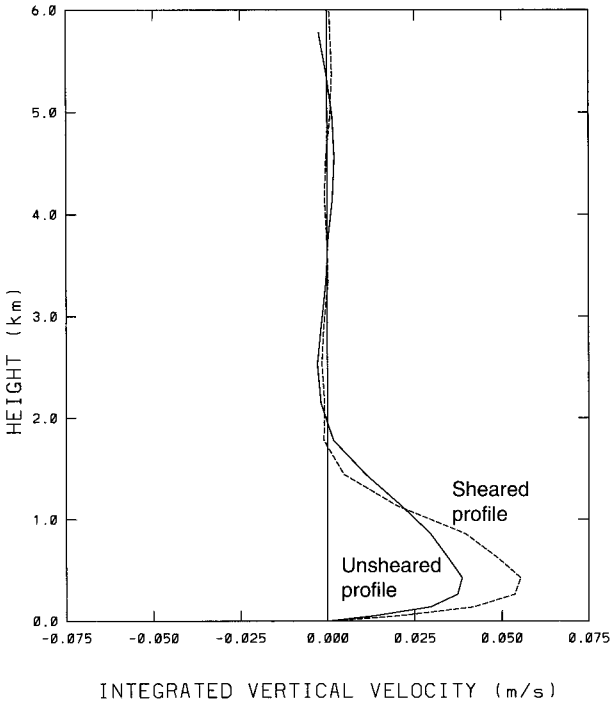

FIG. 6. Profile of mean vertical velocity above the islands for the control experiment, which uses the velocity profile shown in Fig. 3 (dashed line), and an experiment that uses a uniform upstream flow of 4 m s^{-1} (solid line).

of height (Fig. 6). The mean vertical velocity reaches a maximum of 5.5 cm s^{-1} at a height of 500 m, which is approximately the midlevel of the boundary layer. Also plotted in Fig. 6 is the mean vertical velocity from the simulation with no shear. As can be seen, the maximum lifting is reduced by approximately 30% in the case without large-scale shear. The increased lifting in the sheared case is most likely due to trapping of gravity wave energy by the critical level in this simulation (at $z = 1800$ m).

We now examine the sensitivity of this large-scale lifting field to surface heating and to the wind speed and direction. Plotted in Fig. 7a is the mean vertical velocity at 1100 LT as a function of the surface heating rate. As expected from the results of the linear model, the mean vertical velocity shows an approximate linear dependence on the heating rate.

Figure 7b shows the vertical velocity as a function of surface flow speed. Curves are plotted for cases with shear (thick contour) and without (thin contour). For both cases, the integrated vertical velocity decreases with increasing surface flow speed. Also plotted in Fig. 7b is the mean vertical velocity predicted by the linear model. As can be seen, there is reasonable agreement between the linear and nonlinear predictions for flow speeds greater than 4 m s^{-1}. However the curves diverge significantly for flow speeds less than 4 m s^{-1} indicating that nonlinear effects become important at these speeds. The linear model also has a singularity at $U = 0$ whereas

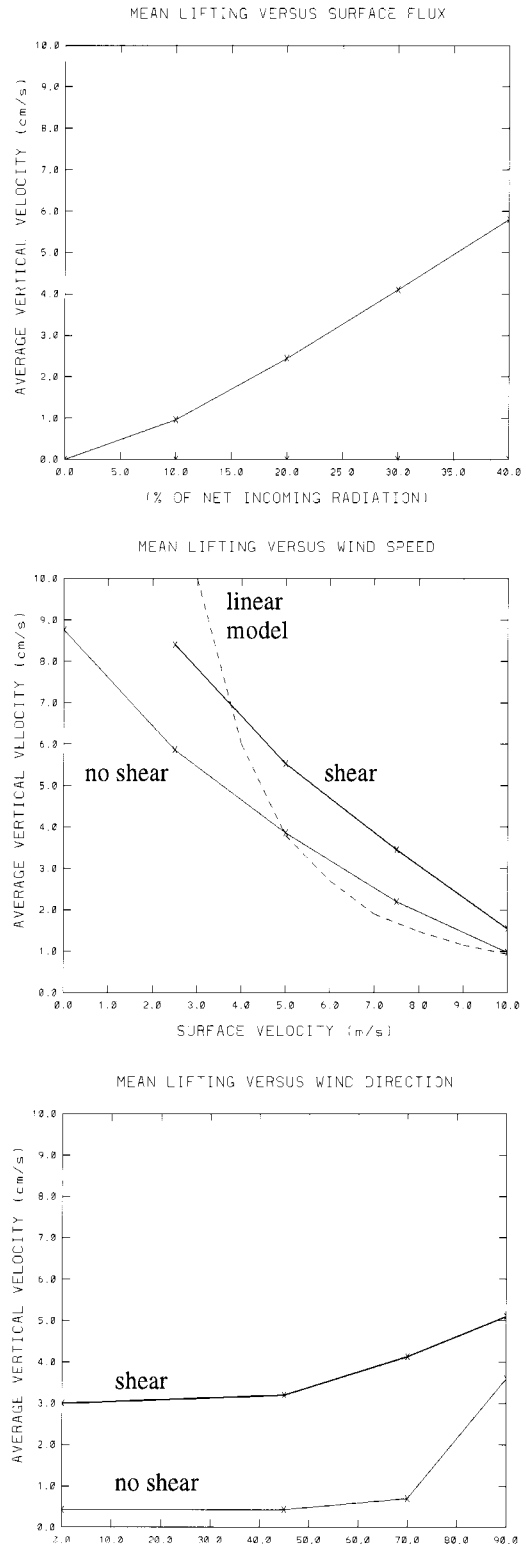

FIG. 7. Average vertical velocity above the islands at $t = 1100$ LT as a function of (a) surface heating rate, (b) wind speed, and (c) wind direction. In (a) the heating rate is given as a percentage of the incoming solar radiation. In (b) the thin contour is for an unsheared flow, the thick contour for a sheared flow, and the dashed contour is the prediction of the linear model. In (c) the thin contour is for an unsheared flow and the thick contour for a sheared flow.

the nonlinear solution in the no shear simulation is bounded at zero flow speed (with an integrated vertical of velocity of 8.8 cm s^{-1}).

During MCTEX, all days with strong thunderstorms had surface winds with speeds less than 4 m s^{-1} (Carbone et al. 2000), placing the flow in a regime where nonlinear effects are important. Hence, although the nonlinear simulations do show that the lifting decreases with increasing flow speed, it is unreasonable to expect a closer agreement with the linear model in this regime.

Figure 7c shows the vertical velocity as a function of surface flow direction. Again, curves are plotted for cases with shear (thick contour) and without (thin contour). For both cases, the integrated vertical velocity is greatest when the flow is toward the east (90°) and decreases as the flow direction turns toward the north. Hence, the numerical simulations are in qualitative agreement with the linear model, which showed that the lifting is greatest when the flow is along the major axis of the islands.

b. Simulations with moisture

1) CONTROL SIMULATION

The previous section has described the development of large-scale convergence over the islands; in this section we examine how that convergence generates moist convection. The control simulation of the previous section is repeated with the moisture profile shown in Fig. 3a added. The surface latent heat flux is set at 40% of the incoming solar radiation. The evolution of the flow is shown in a series of panels in Fig. 8. The surface velocity vectors and cloud water field (z = 1.0 km) at 1000 LT are plotted in Fig. 8a. Sea breezes from the north and south coastlines are shown by the onshore flow and cloud lines along the leading edges. Some clouds have also formed in the interior of the islands. An hour and half later (1130 LT) the two sea breezes have moved farther inland (Fig. 8b). The speed of propagation of the two sea breezes at this time is approximately 1.5–2.0 m s^{-1}. Overlaid on Fig. 8b is the rainwater field at z = 1.0 km. A number of small showers have formed along the two sea breezes and some rain is reaching the surface at this time. At the eastern (downwind) end of Melville Island, there is evidence of cells merging together to form a larger storm complex.

The surface rainwater and velocity field at 1300 LT is shown in Fig. 8c. The north and south sea breezes have propagated farther inland and are now approximately 15 km apart. An east–west line of rainshowers has developed over Melville Island, with the strongest activity at the eastern end. Associated with this convection is an intense gust front (shown by the solid contour) with easterly wind speeds that reach 10 m s^{-1}. One hour later (1400 LT, Fig. 8d) the convective activity has moved farther east and is located near the center of Melville Island. The convection has developed into one

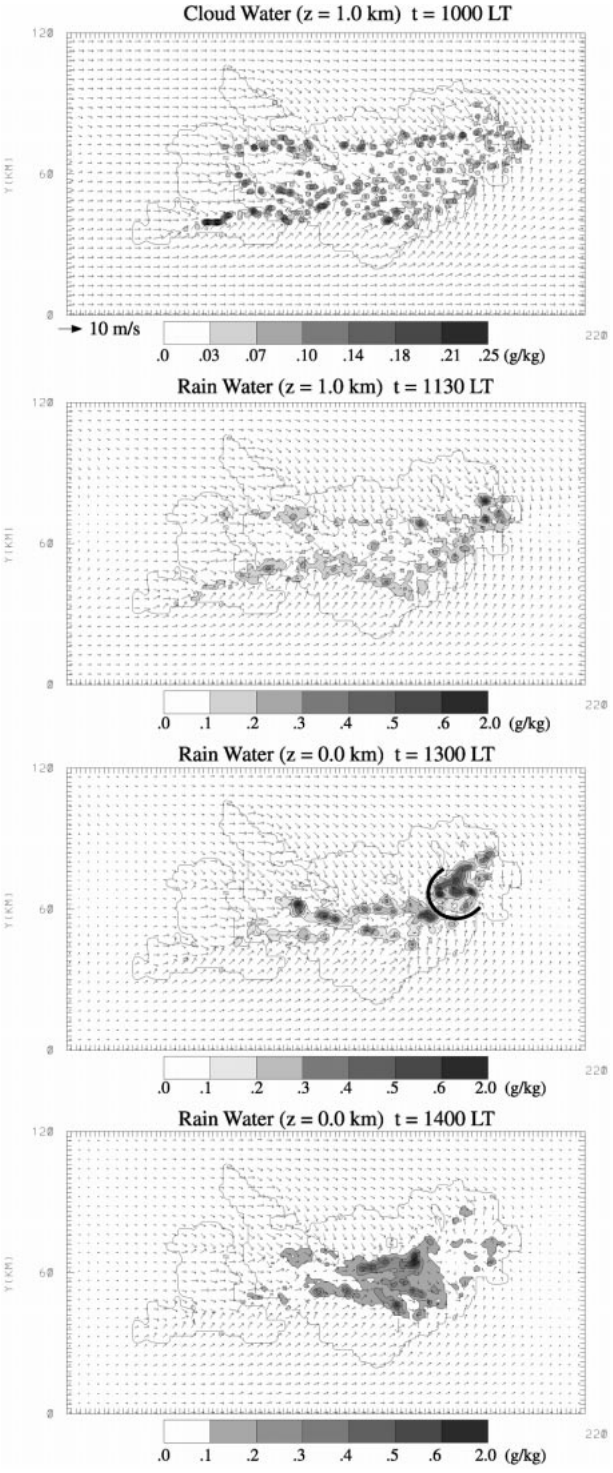

FIG. 8. Evolution of the control experiment with moisture. (a) Cloud water field at z = 1.0 km (t = 1000 LT), (b) rainwater field at z = 1.0 km (t = 1130 LT), (c) surface rainwater field (t = 1300 LT) (gust front with 10 m s^{-1} surface winds is shown by the solid line), and (d) surface rainwater field (t = 1400 LT).

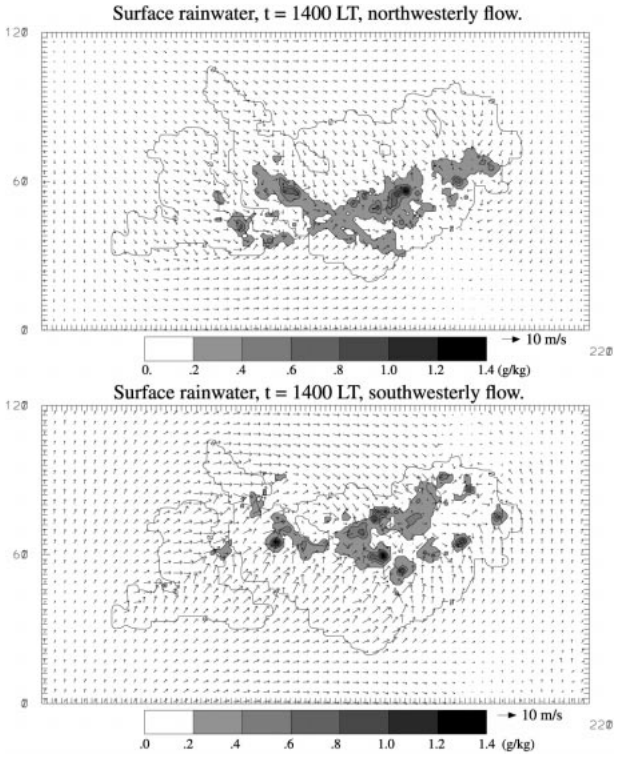

FIG. 9. (a) Surface rainwater and vector fields for (a) low-level northwesterly winds and (b) low-level southwesterly winds.

fairly large cell with horizontal dimensions of approximately 40 km and vertical velocities in excess of 35 m s^{-1}, which places it in the regime of a Hector of moderate size.

2) SENSITIVITY TO WIND DIRECTION

We now examine the sensitivity of convective strength to a number of environmental parameters. The first parameter is the low-level wind direction. In the control simulation, the low-level flow is westerly, which means that there is no preference for convective development along the northern or southern sea breezes. This can be changed by turning the low-level flow so that the sea breeze on the downwind coastline becomes dominant. Figure 9 shows the surface rainwater and flow fields for cases with low-level northwesterly winds (panel a) and low-level southwesterly winds (panel b). With northwesterly winds the major convection occurs along the southern (downwind) sea breeze. With southwesterly winds, the major convection occurs along the northern sea breeze.

Two measures of convective strength are calculated from the simulations. The first is the accumulated rainfall over the islands, which gives a measure of the time-integrated strength of convection over the islands. The second is the maximum value of the total condensate (sum of the cloud, rain, ice A and ice B categories) that occurs during the simulation. This measure gives a better sense of the time-instantaneous strength of convection.

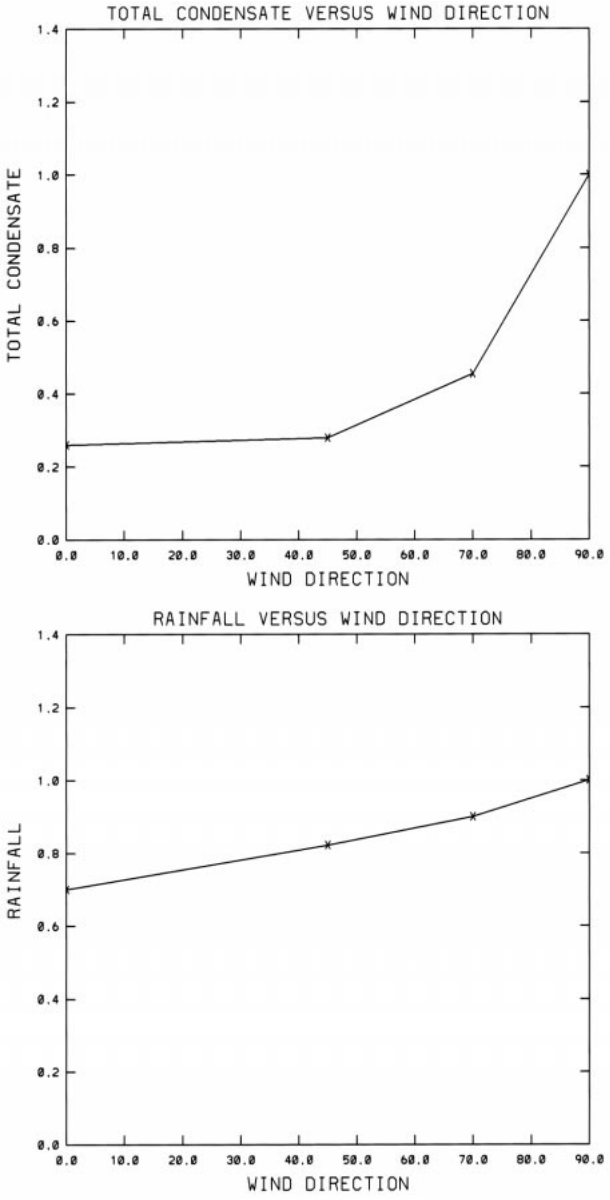

FIG. 10. (a) Total condensate vs wind direction. (b) Accumulated rainfall vs wind direction. Both measures are normalized by the control value.

The accumulated rainfall and total condensate are plotted against the low-level wind direction in Fig. 10. Both measures are normalized by the values that occur in the control simulation. As can be seen, the accumulated rainfall and total condensate maximize for westerly low-level flow (i.e., along the major axis of the island complex). Both measures then drop off monotonically as the flow turns toward the north (along the minor axis), which is in agreement with the decrease in low-level convergence predicted by the linear and nonlinear dry models. The total condensate is reduced by

60% for flow along the minor axis compared to flow along the major axis, while the accumulated rainfall decreases by only 30%.

As mentioned in the introduction, a complete dynamical explanation of the dependence of convective strength on low-level convergence is beyond the scope of the present study; hence, we only speculate on the reason why the accumulated rainfall is less sensitive to the wind direction than the total condensate. When the flow is along the major axis, the low-level convergence is maximized, which leads to the development of an intense convective system (and hence a large total condensate). However the convective system is short lived as the sea breezes from the north and south coastline converge and shut off the supply of unstable air (which leads to a reduced rain accumulation). When the flow is along the minor axis of the island the reduced low-level convergence leads to much weaker convection (as shown by the reduced total condensate). However, the convection lasts longer since the sea breezes from the lateral coastlines do not interrupt the supply of convectively unstable air. Hence the accumulated rainfall does not drop off as quickly as the total condensate as the wind direction turns toward the minor axis of the islands.

3) SENSITIVITY TO WIND SPEED

In Fig. 11, the accumulated rainfall and total condensate are plotted against the low-level wind speed (for westerly flow). Above 4 m s^{-1}, both measures increase as the flow decreases in agreement with the increase in low-level convergence predicted by the linear and nonlinear dry models. However, the convective strength does not continue to increase as the flow decreases below 4 m s^{-1}. Simulations with the dry nonlinear model indicated that the low-level convergence does increase in this flow regime (Fig. 7b). The fact that the convective strength does not continue to increase indicates that the relationship between convective strength and low-level convergence predicted by the linear and nonlinear dry models is not strictly monotonic. This is not surprising for a highly nonlinear phenomenon such as moist convection; however, the mechanism that produces this nonmonotonicity is currently not clear.

One of the nonlinearities in the island thunderstorm problem is the fact that the magnitude of convective instability depends on the flow speed. As the flow speed decreases, the low-level air spends more time over the heat and moisture source provided by the island, and hence the conditional instability at the downwind end of the island is increased. To adjust for this nonlinearity a further set of simulations was performed in which the upwind temperature and moisture profiles for simulations with low-level flow speeds greater than 2 m s^{-1} were modified so as to give profiles at the downwind end of the island that were similar to the profiles from the 2 m s^{-1} simulation. The convective strength for these

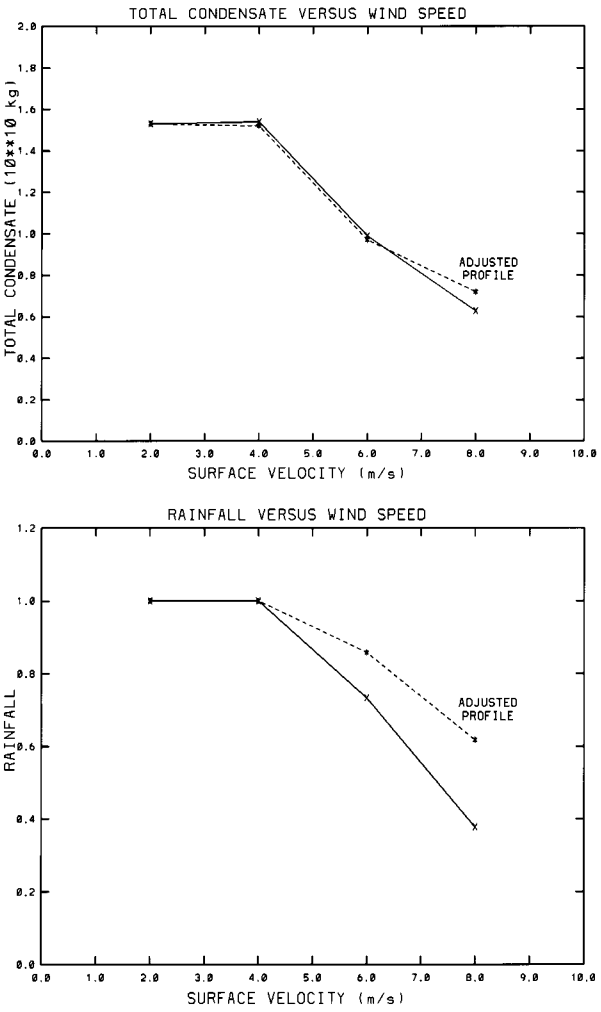

FIG. 11. (a) Total condensate vs wind speed. (b) Accumulated rainfall vs wind speed. The dashed line is for experiments where the upstream sounding is adjusted in order to give a sounding at the downwind end of the island, which is similar to the 2 m s^{-1} simulation.

adjusted simulations is shown by the dashed lines in Fig. 11. The first point to note is that the change in convective strength at 4 m s^{-1} is insignificant. This is because the adjustment to the upstream profile was small since the low-level air spends most of the time over the heat source in this simulation. The second point to note is that total condensate in these modified simulations is not changed significantly, and is still decreasing as the flow increases. The effect on the accumulated rainfall is greater, with the accumulation increasing by 17% at 6.0 m s^{-1} and 60% at 8 m s^{-1}. However, the accumulated rainfall still shows the trend of decreasing convective strength with increasing wind speed shown in the unmodified simulations.

4) SENSITIVITY TO SENSIBLE/LATENT HEAT FLUX

Figure 12 shows the sensitivity of the convective strength to the surface fluxes of heat and moisture. These

sensitivity tests were conducted by varying one of the fluxes while keeping the other fixed (at 40% of the incoming solar radiation). As expected, an increase in either flux leads to an increase in convective strength. However, both measures of convective strength (accumulated rainfall and total condensate) are more sensitive to the sensible heat flux than the latent heat flux. This is not surprising since the low-level convergence that generates the convection is driven by the surface heat flux. This can be seen by the fact that convection does not develop if the surface heat flux is set to zero, whereas there is still some convective development at zero latent heat flux.

5) Sensitivity to low-level moisture

Finally, we examine the sensitivity of convective strength to the low-level moisture (moisture below 1500 m).[1] Figure 13a shows the sensitivity of the accumulated rainfall and the total condensate to the low-level moisture (plotted in terms of the CAPE of the sounding). As can be seen, the accumulated rainfall increases monotonically as the low-level moisture increases. The sensitivity to low-level moisture is strong with the accumulated rainfall increasing by approximately a factor of 2, when the CAPE of the sounding is doubled (from 1500 to 3000 J kg^{-1}). However, Keenan et al. (2000) found only a weak correlation between rainfall and CAPE from the 28 days of MCTEX. There are a number of possible reasons why only a weak correlation was found during MCTEX. These include the small sample size of the MCTEX dataset, the difficulty in determining the upstream CAPE from a single sounding taken over the Tiwi Islands, and the fact that other parameters that the rainfall is sensitive to (such as wind speed and direction, surface fluxes, external forcing, etc.) also varied during the field program.

Figure 13b shows that the total condensate reaches a maximum at a CAPE of around 1500 J kg^{-1} (surface moisture 20 g kg^{-1}) and then slowly decreases thereafter. The reason for this local maximum appears to be that the convection does not organize as well at higher values of low-level moisture. Figure 14 shows the surface rainfall at 1400 LT for a simulation with a CAPE of 3000 J kg^{-1}. The two sea breezes have stalled in this simulation with a separation of approximately 30 km. Consequently, the rainfall is distributed more widely across the islands compared with the control simulation at the same time (Fig. 8d).

The reason that the two sea breezes do not converge

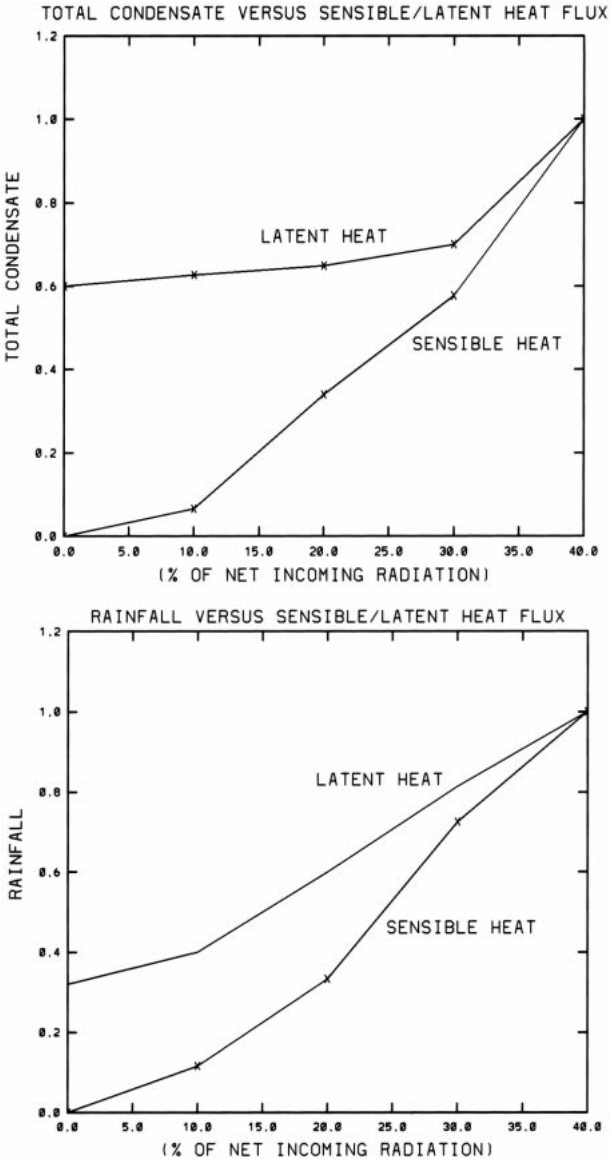

FIG. 12. (a) Total condensate vs sensible and latent heat flux. (b) Accumulated rainfall vs sensible and latent heat flux.

at higher values of surface moisture is that the convection is generated earlier and evaporatively generated cold pools retard the farther inland progression of the sea breezes. This can be seen in Fig. 15, which is a time series of the total condensate for simulations with surface moisture of 18.2 g kg^{-1}, 19.8, and 21.0 g kg^{-1} (CAPE of 1000, 1500, and 3000 J kg^{-1}, respectively). At 21.0 g kg^{-1}, convection commences about 2 h earlier than in the control simulation. This is not surprising, since the convective inhibition of the sounding has decreased significantly (from 47 to 20 J kg^{-1}) and less lifting is required to produce convection.

To show that evaporatively produced cold pools retard the inland progression of the sea breezes, the simulation with the highest surface moisture was repeated with the

[1] It should be noted that varying the low-level moisture changes both the CAPE and the convective inhibition of the sounding. It is possible to vary just the CAPE of the sounding by fixing the low-level moisture and varying the lapse rate above the level of free convection. However, the observations from MCTEX indicate that the day to day variability in CAPE was primarily due to variability in low-level moisture rather than the upper-level temperature.

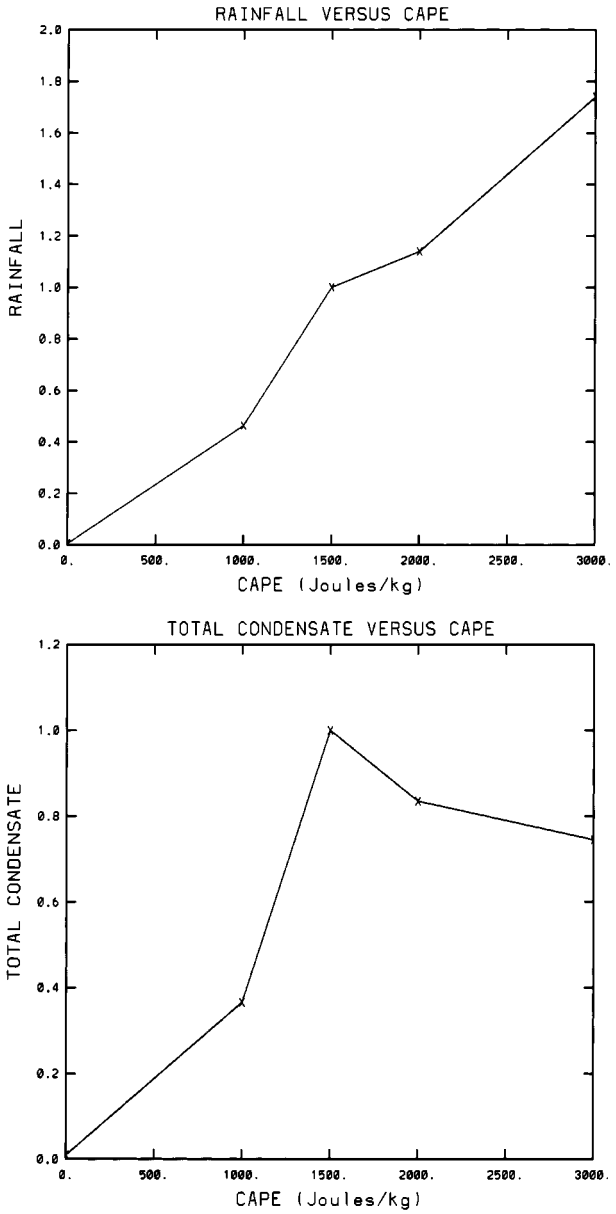

FIG. 13. (a) Accumulated rainfall vs the CAPE of the upstream sounding. (b) Total condensate vs CAPE.

evaporative cooling turned off. Figure 16 shows the surface vector and rainwater field at $t = 1400$ LT. Without evaporatively driven cold pools to impede their progress, the two sea breezes have converged along the east–west centerline of the two islands. The rainfield maximizes along the islands' centerline in contrast to the simulation with evaporative cooling where the rainfield maximizes along two lines where the sea breezes converge with the cold pools.

It is interesting to note that both the accumulated rainfall and total condensate increase significantly when the evaporative cooling is turned off. The accumulated rainfall increases by a factor of 4.7 while the total condensate increases by a factor of 5.8. It is not surprising that the accumulated rainfall increases since the rain does not evaporate at low levels. However, the fact that the total condensate also increases indicates that the convection over a heat island is more efficient without the disruptive influence of evaporatively produced cold pools.

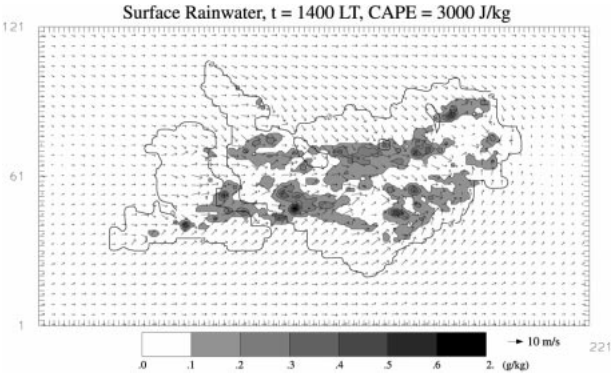

FIG. 14. Surface rainwater and vector field at $t = 1400$ LT for experiment with a CAPE of 3000 J kg^{-1}.

6) TYPE A VERSUS TYPE B CONVECTION

In this study we have primarily concentrated on the integrated convective response to island forcing rather than the details of the convective structure. As mentioned in the introduction, one of these details in structure is the difference between type A and type B modes of development discussed in Carbone et al. (2000). The simulations presented herein suggest that the parameter that is most important for determining whether the con-

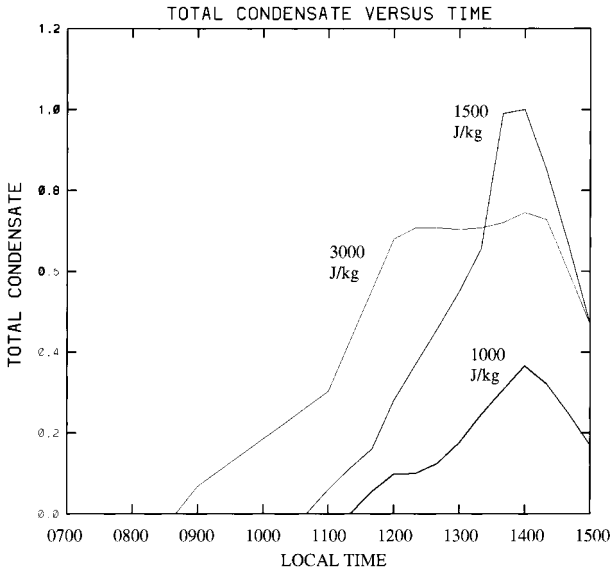

FIG. 15. Total condensate against time for simulations with upstream CAPEs of 1000, 1500, and 3000 J kg^{-1}. All measures are normalized by the maximum value from the control experiment.

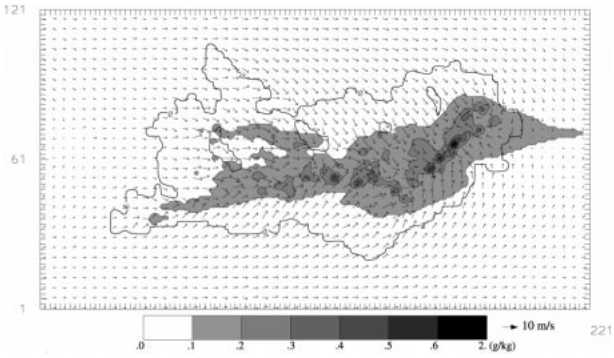

FIG. 16. Surface rainwater and vector field at $t = 1400$ LT for an experiment with a CAPE of 3000 J kg^{-1} and with evaporation turned off. To be compared with Fig. 14.

vection is of type A or B is the low-level moisture. A similar conclusion was drawn from the MCTEX dataset by Carbone et al. (2000). Before convection develops, the inland progression of the sea breezes is controlled largely by the surface heat flux and the low-level flow conditions. However, at higher values of low-level moisture, convection is generated earlier and evaporatively produced cold pools then retard the farther inland progression of the sea breezes. Subsequent convective development then occurs between the sea breezes and the evaporatively produced cold pools. At lower values of moisture, the generation of evaporatively produced cold pools is delayed so that the sea breezes have time to converge. Convection will then be generated between the converging sea breezes as long as the intervening air has positive CAPE.

As discussed above, type B convection occurs between a single sea breeze and a cold pool produced by previous convection. An interesting question then is whether convection of similar strength can be generated along a sea breeze from a single coastline in the absence of a nearby coastline. In other words, could similar strength convection be generated along the coastline of a continent where the influence from the opposite coastline is negligible. To answer this question, both the linear and nonlinear models were run for a landmass that had only a northern coastline as shown in Fig. 17. For the linear model the northern coastline was assumed to be half of an ellipse, while the nonlinear model uses the northern coastline of the Tiwi Islands. The linear response, shown in Fig. 17a, indicates that the large-scale convergence is decreased by approximately a factor of 2 for this continental landmass (cf. with Fig. 1a). This is not surprising since the circulation is forced by only one land–sea contrast instead of two. Figure 17b shows the nonlinear response along with the surface rainwater field. Some convection is generated along the sea breeze but it is insignificant compared with that which forms over an island. This indicates that the convergence between the sea breeze and cold pools is enhanced by the proximity of the opposite coastline. In other words, one of the main reasons that the Hector convective system is so strong is that it forms over an isolated heat source.

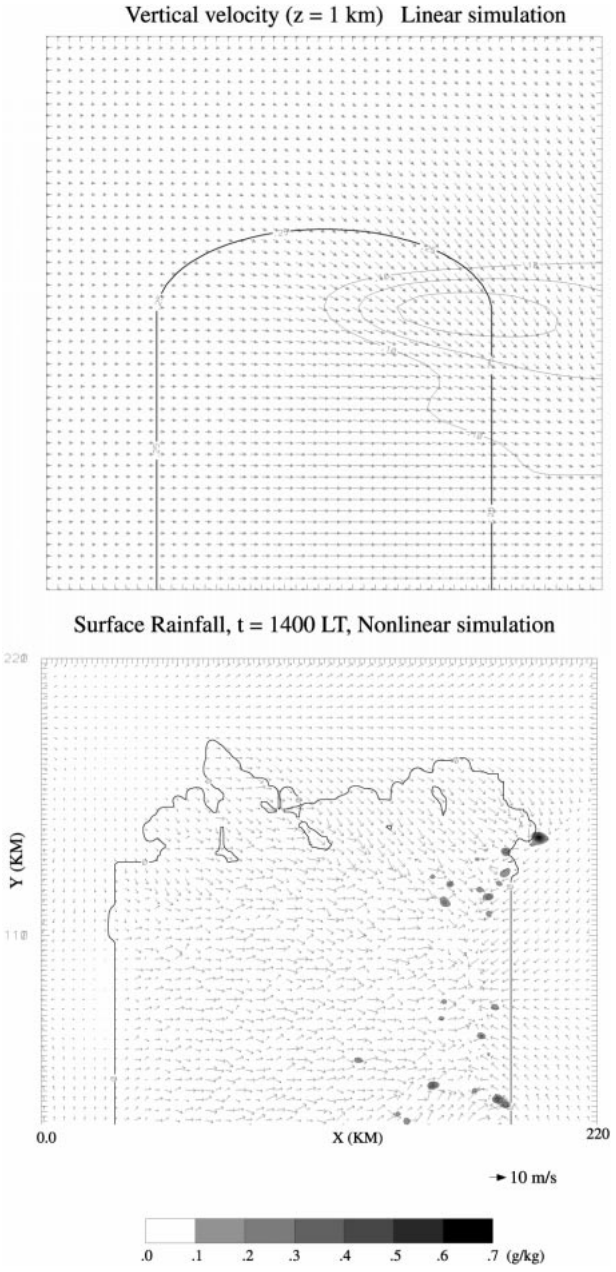

FIG. 17. (a) Surface vectors and vertical velocity at the top of the heat source for linear flow of 4 m s^{-1} past a heat source that has only a northern coastline. To be compared with Fig. 1a. (b) Surface vectors and rainwater field for nonlinear flow of 4 m s^{-1} past a heat source that has only a northern coastline ($t = 1400$ LT). To be compared with Fig. 8d.

4. Summary and conclusions

In this study, we have examined the flow response to an isolated heat and moisture source in order to gain

insight into the development of island thunderstorms. Both linear and nonlinear models have been used to examine this response. The main conclusions of the study are as follows.

1) Linear results: For moderate and high Froude number conditions ($U/NH > 1$) the linear model predicts that the low-level convergence forced by an elliptical heat source is maximized when the flow is weak and along the major axis of the heat source.
2) Nonlinear results: (i) Dry conditions—A dry version of the nonlinear model verified the trends predicted by the linear model except at very low flow speeds where the convergence was bounded in the nonlinear model but increases indefinitely in the linear model. (ii) Moist conditions. An intense convective system, similar to that observed over the Tiwi Islands, was simulated with a moist version of the nonlinear model. The dependence of the convective strength on the wind speed and direction, surface fluxes, and low-level moisture was then examined. It was shown that the convective strength increases as the wind speed decreases and as the wind direction turns toward the major axis of the island, in agreement with the prediction from the linear and nonlinear models. The one exception to this general result was for flow speeds less than 4 m s^{-1} where the convective strength did not continue to increase as the wind speed decreased.

The nonlinear model showed that the convective strength increases as both the heat and moisture fluxes increase. The strength was more sensitive to the heat flux since this drives the large-scale convergence and sea breezes that generate the convection.

The accumulated rainfall over the islands increases monotonically as the low-level moisture increases. However, the total condensate reaches a maximum at a CAPE of around 1500 J kg^{-1} and then decreases thereafter. At higher values of surface moisture, the convection is more widespread and less organized and efficient. It was also shown that the parameter that differentiates between the type A and Type B modes of convection is the low-level moisture. At higher values of surface moisture, convection is generated earlier and evaporatively produced cold pools retard the farther inland progression of the sea breezes. Further convection then develops between the sea breezes and the cold pools (type B). When the CAPE is low but still positive, the generation of convection is delayed until the sea breezes converge near the center of the island (type A).

Finally, the question of island versus continental convection was examined by running a simulation with a single coastline. The convective strength in this simulation was diminished significantly suggesting that one of the reasons the Hector convective system is so strong is that it develops over an isolated heat source where convergence is generated by two nearby coastlines. This raises the question of what is the optimal size for an island to produce the most intense convection. If the island is too large, then the influence from the other coastline is diminished. However, if the island is too small then the flow does not have enough residence time over the island to produce convergence or conditional instability. The question of optimal island size was addressed briefly by Saito et al. (2001) although no firm conclusions were drawn. Thus, a quantitative investigation of this question remains to be performed.

Acknowledgments. Reviews of an earlier version of this paper by J. Wilson and R. Carbone are gratefully acknowledged.

REFERENCES

Beringer J., N. Tapper, and T. Keenan, 1997: Surface energy balance measurements over the Tiwi Islands, Northern Territory, Australia, during the Maritime Continent Thunderstorm Experiment (MCTEX). Preprints, *22d Conf. on Hurricanes and Tropical Meteorology*, Fort Collins, CO, Amer. Meteor. Soc., 374–375.

Carbone, R. E., J. W. Wilson, T. D. Keenan, and J. M. Hacker, 2000: Tropical island convection in the absence of significant topography. Part I: Life cycle of diurnally forced convection. *Mon. Wea. Rev.*, **128,** 3459–3480.

Clark, T. L., 1977: A small scale numerical model using a terrain following coordinate transformation. *J. Comput. Phys.*, **24,** 186–215.

——, and R. D. Farley, 1984: Severe downslope windstorm calculations in two and three dimensions using anelastic interactive grid nesting: A possible mechanism for gustiness. *J. Atmos. Sci.*, **41,** 329–350.

Golding, B. W., 1993: A numerical investigation of tropical island thunderstorms. *Mon. Wea. Rev.*, **121,** 1417–1433.

Keenan, T., and Coauthors, 2000: The Maritime Continent Thunderstorm Experiment (MCTEX): Overview and some results. *Bull. Amer. Meteor. Soc.*, **81,** 2433–2455.

Kessler, E., 1969: *On the Distribution and Continuity of Water Substance in Atmospheric Circulations. Meteror. Monogr.*, No. 32, Amer. Meteor. Soc., 84 pp.

Koenig, L. R., and F. W. Murray, 1976: Ice-bearing cumulus cloud evolution: Numerical simulation and general comparison against observations. *J. Appl. Meteor.*, **15,** 747–762.

Lilly, D. K., 1962: On the numerical simulation of buoyant convection. *Tellus,* **14,** 148–172.

Lin, Y.-L., 1986: Calculation of airflow over an isolated heat source with application to the dynamics of V-shaped clouds. *J. Atmos. Sci.*, **43,** 2736–2750.

Malkus, J. S., and M. E. Stern, 1953: The flow of a stable atmosphere over a heat island. Part I. *J. Meteor.*, **10,** 30–41.

Raymond, D. J., 1972: Calculation of airflow over an arbitrary ridge including diabatic heating and cooling. *J. Atmos. Sci.*, **29,** 837–843.

Saito, K., T. Keenan, G. Holland, and K. Puri, 2001: Numerical simulation of the diurnal evolution of tropical island convection over the Maritime Continent. *Mon. Wea. Rev.*, **129,** 378–400.

Skinner, T., and N. Tapper, 1994: Preliminary sea breeze studies over Bathurst and Melville Islands, Northern Australia, as part of the Island Thunderstorm Experiment (ITEX). *Meteor. Atmos. Phys.*, **53,** 77–94.

Smagorinsky, J., 1963: General circulation experiments with the primitive equations. I: The basic experiment. *Mon. Wea. Rev.*, **91,** 99–164.

Smith, R. B., and Y.-L. Lin, 1982: The addition of heat to a stratified airstream with application to the dynamics of orographic rain. *Quart. J. Roy. Meteor. Soc.*, **108,** 353–378.